NASA TECHNICAL NOTE

NASA TN D-3256

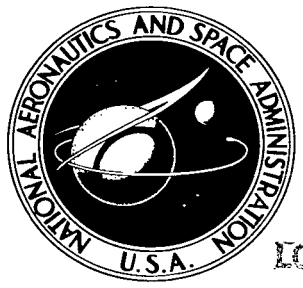

NASA TN D-3256

WALL AND BOTTOM HEATING OF LIQUID HYDROGEN IN A PROPELLANT TANK

by Sidney C. Huntley, James W. Gauntner, and Bernhard H. Anderson

Lewis Research Center
Cleveland, Ohio

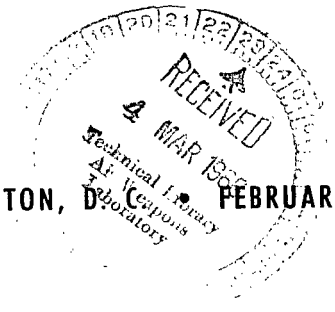

NATIONAL AERONAUTICS AND SPACE ADMINISTRATION • WASHINGTON, D. C. • FEBRUARY 1966

NASA TN D-3256

WALL AND BOTTOM HEATING OF LIQUID HYDROGEN IN A PROPELLANT TANK

By Sidney C. Huntley, James W. Gauntner, and Bernhard H. Anderson

Lewis Research Center
Cleveland, Ohio

NATIONAL AERONAUTICS AND SPACE ADMINISTRATION

For sale by the Clearinghouse for Federal Scientific and Technical Information
Springfield, Virginia 22151 – Price $2.00

WALL AND BOTTOM HEATING OF LIQUID HYDROGEN IN A PROPELLANT TANK

by Sidney C. Huntley, James W. Gauntner, and Bernhard H. Anderson

Lewis Research Center

SUMMARY

An experimental investigation was made to determine the behavior of liquid hydrogen in a 125-gallon scale model of a propellant tank subjected to a range of wall heat flux from 0.0012 to 0.0082 Btu per square foot per second and a range of bottom heat flux from 0.0005 to 0.0098 Btu per square foot per second while discharging from the tank at a rate of 0.04 pound per second under a constant tank pressure of about 2 atmospheres. Increasing temperature stratification in the liquid was encountered with increasing wall heat flux; a decrease in stratification was experienced with increasing bottom heat flux. An available analysis partially predicted the increase in temperature stratification.

Generalization of the exit temperature histories showed that the data were applicable to other test conditions provided similarity existed in the normalized heat input rate distribution. Application of the generalization method to other test data showed that bottom heating gave results similar to nuclear heating from below which had a similar overall heat input rate distribution.

No gross changes in liquid behavior were experienced over the range of experimental conditions.

INTRODUCTION

A knowledge of the effect of heat leaks into the cryogenic propellant in a vehicle storage tank is required for the optimization of tank pressurization, tank insulation, and residual propellant requirements of the vehicle. In chemical rockets, thermal radiation and aerodynamic heating supply a net influx of heat to the propellant from the tank walls. In nuclear rockets, additional heating of the fluid arises from the absorption of neutron and gamma ray radiation both in the tank walls and in the fluid. This heating of the fluid produces both an increase in the bulk temperature and a vertical temperature gradient (stratified layer) near the liquid surface. In the case of constant pressure discharge, the significance of the stratified layer is realized when a pump is used in the propellant

feed system. The net positive suction head requirements of the pump limits the permissible temperature rise in the subcooled liquid. Thus a portion of the stratified layer represents unusuable propellant, the quantity of which must be minimized. The amount of unusable propellant depends on the heat influx to the tank, both magnitude and distribution, which in turn is determined by the thermal protection of the vehicle tank and the flight environmental conditions.

Numerous experimental and analytical studies have examined the problems associated with the storage of cryogenic propellants under the conditions of external heat loads. Experimental measurements on the transient temperature distribution in the liquid are presented in references 1 and 2. These data were obtained under no-flow conditions. A number of approximate analyses have been developed to predict transient temperature profiles in the fluid proper for closed tanks and tanks with outflow. Typical examples of this work are presented in references 3 to 5. A visual study of the flow behavior of a noncryogenic fluid in a small two-dimensional vented tank was reported in reference 6. The stratification pattern was examined when the liquid heating was from the side walls, bottom, or internal absorption of energy or a combination thereof. Infrared radiation was used as a heat source. The results indicated that the stratification pattern is very dependent on the mode of heating. An excellent review article which discusses and summarizes both experimental and analytical work done in this field appears in reference 7. A series of tests was conducted under contract to obtain data with wall and bottom (including source) heating of liquid hydrogen provided by a nuclear environment (ref. 8). Tests were conducted in a 125-gallon tank in which the flow rate, total heating rate, and tank pressure were varied. It should be noted that although the total heating rate could be varied, there was no provision for separately controlling the side wall heating. Presented in reference 9 is a comparison between an analysis and results from the nuclear environment tests. The analysis was developed in reference 9 primarily to predict the transient temperature distribution in liquid hydrogen with wall and nuclear heating for conditions of constant pressure discharge.

To further study the liquid behavior over a wider range of heating rate distribution, a series of experiments was conducted at the Lewis Research Center with liquid hydrogen in a 125-gallon tank similar to that used in the nuclear environment tests. This series of tests used separately controlled radiant heaters located along the side and bottom of the tank to permit variation of both side and bottom heating. It is the purpose of this report to document the results of this series of tests. The analysis presented in reference 9, giving general agreement with the experimental nuclear data, was applied to the present series of tests and its range of applicability is briefly discussed. A set of nondimensional scaling parameters are developed and utilized in the presentation of the experimental data so that they can be made more directly applicable to other test conditions. The generalization was then applied to the results of the nuclear environmental

tests and comparisons are made with the data reported herein.

APPARATUS AND PROCEDURE

The experiment was designed to simulate a rocket vehicle system. The experimental tank and test parameters were chosen by scaling a rocket vehicle tank having a capacity of 100 000 pounds of liquid hydrogen. The value of the flow rate was chosen to yield about the same time to outflow as the full size tank and the tank was pressurized to about 2 atmospheres, which was deemed adequate for typical missions. The test tank used in this series of tests was geometrically the same as the one used in the nuclear environmental tests (ref. 8). This was deemed necessary so that a direct comparison could be made between the results reported herein and those reported in reference 8. The magnitude of the heating rate applied to the tank was chosen to preserve heating loads (heating rate per unit volume of liquid) for typical chemical and nuclear rocket missions for the full-size tank. (Symbols used in this report are listed in appendix A.)

The experimental apparatus is reported in detail in appendix B; thus, only a cursory description is included here. The test apparatus (fig. 1) consisted of a test tank enclosed in a vacuum chamber with provisions for supplying liquid hydrogen, pressurizing and venting the tank, throttling the outflow, and providing separately controlled heating of the tank side wall and bottom. A vacuum system was provided that had the capability of providing a vacuum of less than 10^{-5} torr, thereby reducing the conductive heat leak through the vacuum space to a negligible amount. The outer shell of the vacuum space was provided with liquid nitrogen cooling to reduce the radiant heat flow into the sides and bottom of the test tank. Solar radiation and/or aerodynamic heating was simulated by using electrical radiant heaters (fig. 2) suspended in the vacuum. A detailed description of the radiant heaters is also presented in appendix B.

Two temperature measurement systems were used for the tests: one system consisted of carbon resistor thermometers to measure temperatures in the cryogenic range and the other of copper constantan thermocouples to measure temperatures above the cryogenic level. Temperature data are presented in this report for thermometers located at 0, 16.9, 24.7, 32.7, and 40.7 inches above the exit port along the tank center axis. Other types of measurements included tank pressure, liquid flow rate, and liquid level position.

The flow test conditions for each heating rate distribution considered are presented in table I. Each test is characterized by a different heating rate distribution which is identified by the average wall heat flux relative to the average bottom heat flux; that is, the identification H - L indicates that the average wall heat flux (H) was somewhat higher than the average bottom heat flux (L). Intermediate values of heat flux are

designated as either ML or MH. The initial height of liquid, initial liquid temperature, tank pressure with resulting saturation temperature, and flow rate are also shown. Three types of tests were performed in this investigation: boiloff, no-flow, and flow tests. Detailed operating procedures for each of these tests are presented in appendix B. The boiloff and no-flow (self-pressurizing) tests were used as calibration runs to substantiate the heating rate distribution for the flow tests.

The method of obtaining the heat input distribution for the flow tests was based on a calculation of the net radiant heat exchange between the radiant heaters and the tank walls. The net heat input rate from the heaters was obtained from the equation

$$\dot{Q}_H(x_s) = \int_0^{x_s} q(x) \frac{dS}{dx} dx \tag{1}$$

The quantity $q(x)$ is the net heat flux from the radiant heaters (see eq. (C1) of appendix C), S is the wetted surface area of the tank, and x_s is the location of the liquid surface. Because the calculations did not consider other forms of heat transfer that were present (e.g., radiation from the tank dome), independent checks of the heat input were performed and corrections to the heating rate were made. This was accomplished by first integrating the radiant heating rate distribution over the time to outflow for each run. The average heat input rate was established by means of the expression

$$\dot{\bar{Q}}_H = \frac{1}{t_m} \int_0^{t_m} \int_0^{x_s(t)} q(x) \frac{dS}{dx} dx\, dt \tag{2}$$

The average heating rate of the liquid for each run was obtained by the integration of the temperature history at the exit port using the equation

$$\dot{\bar{Q}}_\ell = \frac{\overline{\rho c_p} \dot{V}}{t_m} \int_0^{t_m} \Delta T(o, t)\, dt \tag{3}$$

where the density $\bar{\rho}$ and specific heat at constant pressure $\bar{c}_p$ were evaluated at the average temperature over the time to outflow defined by the expression

$$\bar{T} = T_{in} + \frac{1}{t_m} \int_0^{t_m} \Delta T(o, t)\, dt$$

and $\dot{V}$ is the average volumetric flow rate calculated from the slope of a straight-line curve fit of liquid volume history. The liquid volume history was obtained by observing the time at which the liquid surface passed the several temperature sensor locations.

The average heating rate from the heaters $\bar{\dot{Q}}_H$ and the average heating rate of the the liquid $\bar{\dot{Q}}_\ell$ thus obtained were then used as a basis for adjusting the calculated radiant heat distribution by means of the equation

$$\dot{Q}_\ell(x) = \frac{\bar{\dot{Q}}_\ell}{\bar{\dot{Q}}_H} \dot{Q}_H(x) \tag{4}$$

The value of $\bar{\dot{Q}}_\ell / \bar{\dot{Q}}_H$ obtained for each flow test is shown in table I. In order to establish the validity of this adjustment, independent checks of the total heating rate $\dot{Q}_\ell(L)$ and the heating rate distribution $\dot{Q}_\ell(x)$ were made using boiloff and no-flow tests. A detailed discussion of the heating calculations and the methods of substantiating these calculations appears in appendix C.

The heating rate distribution (eq. (4)) and the flow test conditions (table I) for each heating configuration were used as input for the analysis developed in reference 9 and the liquid temperature history was calculated. A detailed discussion of the method of application and the basic equations used in the analysis is presented in appendix D.

TEST RESULTS

Several flow tests were conducted in which the side wall and bottom heat flux were held constant. Each test had a different heating configuration distinguished by the relative values of wall and bottom heat flux (table I). The tests were conducted primarily to show the effect of varying wall or bottom heat flux on the behavior of liquid hydrogen during constant pressure discharge. Heat input rate distributions obtained from the flow test experiments are given, followed by the presentation of the experimental temperature histories and a comparison between the experimental results and analytical predictions.

Heat Input Distribution

The heat input rate from the heaters is presented in figure 3 as a function of liquid height for the several configurations. Data points represent calculated values of heat input rate using equation (1). Solid curves are used to depict test configurations related

by having increasing values of wall heat flux, while the dashed curves depict increasing values of bottom heat flux. The lowest curve represents the condition of minimum heat leak to the tank obtained with no power supplied to the heaters; the top curve was obtained with both heaters giving about equal heat fluxes, such that the bulk of liquid was heated to saturation by the time the tank was emptied.

Time-averaged heating rates in the liquid and from the heaters are presented in figure 4 for the several heating configurations. The quantity $(\dot{\bar{Q}}_\ell - \dot{\bar{Q}}_H)/\dot{\bar{Q}}_H$ defined as the heating error is shown as a function of the average heating rate from the heaters. Also shown are the results obtained from the no-flow tests described in appendix C. The dashed curves represent constant $\dot{\bar{Q}}_\ell - \dot{\bar{Q}}_H$ values of 15 and 30 watts. The data for the two types of tests show good general agreement although the heating error was greater for the no-flow type of tests.

Experimental Temperature Histories

The temperature history at several axial locations in the tank is presented in figure 5 for each heating configuration (see table I for initial conditions). The experimental data are depicted by solid curves; the dashed curves, which show predicted temperature histories, will be discussed in the next section. In general, the temperature at a given location rises gradually with time during the outflow of liquid from the tank. The rapid increase in temperature indicates the presence of a stratified layer of warm liquid near the surface. The nearly constant temperature after the rapid increase corresponds to saturation temperature. Apparently the dip in the temperature history occurs when the thermometer becomes exposed to the gas and evaporization of the liquid film causes a slight cooling effect.

The data for the L - L configuration which represents the minimum heat input is presented in figure 5(a). Under this heat input condition, the gain in liquid temperature at the exit was small until the tank was nearly empty. The constant temperature at any time for several locations indicates that the heat was distributed uniformly throughout the liquid except near the surface.

The H - H configuration (fig. 5(b)) had the maximum heat input to the tank and was chosen to result in heating the bulk of liquid to saturation temperature just prior to the tank being empty. Comparison of the results of this test with those of the minimum heat configuration (fig. 5(a)) shows that the increase in average heat flux from 2.4×10^{-3} to 8×10^{-3} Btu/per square foot per second resulted in a general increase in liquid temperature at any given time. A measurable axial temperature gradient existed in the liquid with the H - H configuration as is shown by the spread in temperature of several thermometers at a given time.

Comparison of the data for the L - L, ML - L, MH - L, and H - L configurations (figs. 5(a), (c), (d), and (e)) shows the effect of increasing the wall heat flux from approximately 2.8×10^{-3} to 7×10^{-3} Btu per square foot per second with low bottom heat flux. A comparison of the data shows that the exit temperature rise in about the first 300 seconds was approximately the same although wall heat flux was increasing. Since the increase in wall heat flux occurred above a height of about 16 inches from the tank exit (fig. 3), the first 3 cubic feet of liquid to leave the exit would not sense the increase in heat. Therefore, with an outflow rate of about 0.04 pound per second, about 300 seconds should be required before the influence of wall heat is observed at the exit. Increasing the wall heat flux resulted in an increasing rate of exit temperature rise (after 300 sec) except when the tank was nearly empty. The spread in temperature between given locations in the tank increased with increasing wall heat flux at a given time indicating more heat is accumulating in the stratified layer.

A comparison of the data for the L - ML, L - MH, and L - H configurations (figs. 5(f), (g), and (h)) shows the effect of increasing the bottom heat flux from about 3.6×10^{-3} to 9.8×10^{-3} Btu per square foot per second with low wall heat flux. As in the case of variable wall heat flux, increasing the bottom heat flux results in an increasing rate of exit temperature rise but, since the heat is added at the tank bottom, the spread in temperature between thermometers is smaller. The liquid temperature at each location rises at a nearly uniform rate with bottom heating. Apparently increasing the heat at the tank bottom results in increased mixing with the fluid approaching a completely mixed condition except for a thin layer near the liquid surface.

Comparison of Experimental and Predicted Temperature

Predicted temperature histories for each of the experimental heating configurations based on the analysis of reference 9 (see appendix D) are in general agreement with the experimental data (fig. 5). Deviations that occur may be classified into two types: one pertaining to mass and the other to energy. Deviations due to mass occur primarily because of the difference between using an average flow rate in the analysis and the instantaneous flow rates of the experiment. Deviation of the actual from the predicted time for the surface to pass any location in the tank is consequently due to flow rate variations from the average value during a test or to slight differences between actual probe locations and those used in the analysis.

Deviations pertaining to energy refer to the suitability of the analysis to predict the liquid behavior. The predicted temperature history at the tank exit, based on consideration of energy conservation, should prescribe the total input energy to the system. The determination of the input energy, on the other hand, is dependent on both the time-

averaged experimental exit temperature history and the time-averaged volume history. Temperature deviations at the tank exit therefore result from both flow rate variations and the manner in which the analysis distributes the energy input at any time.

Slight deviations pertaining to mass between the experimental data and the analysis result in large temperature deviations because of the rapid temperature rise that occurs as the liquid surface approaches a given sensor location. Temperature deviations of this type appear to be of some consequence but are not considered to be of major significance because refinements of the analytical technique are possible. Of greater interest here are the temperature deviations, between the experimental data and the analysis, pertaining to energy. The analysis prescribes a temperature profile dependent on heat flux distribution along the wetted tank surface and a percentage of the total heating rate which enters the stratified layer. The temperature profile thus established determines the predicted temperature rise at any given location.

A comparison of the predicted and experimental temperature history at several locations for the cases with increasing wall heat flux (L - L, ML - L, MH - L, and H - L, see figs. 5(a), (c), (d), and (e)) shows that deviations in temperature profiles increase with increasing wall heat flux. A similar comparison between cases with increasing bottom heat flux (figs. 5(f), (g), and (h)) indicates the opposite trend. It is apparent that best agreement between the analysis and data is obtained with heat input distributions having relatively high bottom heating. However, the general agreement between the predicted and measured temperature histories indicate the analysis of reference 9 may be useful for interpolation.

GENERALIZATION OF DATA

For experimental data obtained in small tanks to be applicable to a full-scale tank, such tests must simulate the operating conditions prevailing in the environment in which the full-scale system will function. This requirement necessitates the establishment of a set of dimensionless parameters that must have the same value for both the model and the full-scale system. Such a set of dimensionless parameters is derived to obtain generalized temperature histories.

Dimensionless Parameters

Dimensionless parameters are desired to describe the system consisting of the liquid bounded by the tank walls and the liquid gas interface at any time during flow at constant pressure. An energy balance of the system may be expressed in terms of the

time rate of increase in liquid enthalpy, the rate at which enthalpy is being transported from the system, and the heating rate entering the system. When no heat transfer at the interface and no radial temperature gradients are assumed, the energy equation can then be written as

$$\overline{\rho c}_p \frac{d}{dt} \int_{V(x_s)} \Delta T(x, t) dV + \overline{c_p} \dot{w} \, \Delta T(o, t) = \dot{Q}_\ell (x_s) \tag{5}$$

where $\dot{w}$ is the flow rate and $V(x_s)$ is the volume of liquid in the tank at any given time. A saturation heating rate $\dot{Q}_s$ is now defined as the energy required to heat the initial liquid content to saturation temperature in the same time required to empty the tank. This saturation heating rate can be illustrated by means of the expression

$$\dot{Q}_s = \frac{\overline{\rho c}_p V(L) \, \Delta T_s}{t_m} = \overline{c_p} \dot{w} \, \Delta T_s \tag{6}$$

Combining equations (5) and (6) yields the energy equation as

$$\frac{d}{d\tau} \int_{v(x_s)} \vartheta \left(\frac{x}{L}, \tau \right) dv + \vartheta (o, \tau) = \dot{\mathcal{Q}} \frac{\dot{Q}_\ell (x_s)}{\dot{Q}_\ell (L)} \tag{7}$$

where

$$\tau = \frac{t}{t_m}$$

$$v = \frac{V(x)}{V(L)}$$

$$\vartheta = \frac{\Delta T}{\Delta T_s}$$

$$\dot{\mathcal{Q}} = \frac{\dot{Q}_\ell (L)}{\dot{Q}_s}$$

In this form the energy equation states that the nondimensional temperature history everywhere in the tank is a function of the nondimensional heat input rate distribution $\dot{Q}_\ell(x_s)/\dot{Q}_\ell(L)$ and a heating parameter $\dot{\mathcal{Q}}$. The heating parameter $\dot{\mathcal{Q}}$ relates the initial heating rate to the other test conditions of flow rate $\dot{w}$ and tank pressure (in terms of saturation temperature ΔT_s).

Heat Input Rate Distribution

The heat input rates to the liquid, normalized to the initial values of heat input rate, are presented in figure 6 for the several heating configurations. Also shown by the dashed line is a typical total heating distribution curve from the nuclear heating data of reference 8 (this curve will be discussed in a later section).

The generalized heat input rate distribution for the H - H configuration, having been obtained with about constant heat flux, represents the nondimensional tank surface area as a function of x/L (see eq. (1)). Consequently, curves which lie above represent configurations with relatively higher bottom heat flux; those below represent relatively higher wall heat flux.

Increasing the bottom heat flux (L - ML, L - MH, L - H) from 3.6×10^{-3} to 9.8×10^{-3} Btu per square foot per second did not result in as large a change in shape of the generalized heat input rate distribution curve as expected (fig. 6). This was partially due to an increasing wall heat flux with increased bottom heat flux. The heat input rate distribution curves have about the same general shape as the total heating distribution of the nuclear data, which is shown on figure 6 but will be discussed in a later section.

An increase in wall heat flux (L - L, ML - L, MH - L, H - L) from 2.8×10^{-3} to 7×10^{-3} Btu per square foot per second also did not affect the general shape of the distribution curves. In general, the heat input rate distribution curves can be classified into two general shapes, those with high bottom heating and those with high wall heating. This general grouping of the data is used as a convenient basis for the following discussion.

Generalized Exit Temperature Histories

The input to the generalized temperature histories was considered to consist of two parts, $\dot{\mathcal{Q}}$ and $\dot{Q}_\ell(x_s)/\dot{Q}_\ell(L)$. The latter, discussed in the previous section, was shown to consist primarily of two types of heating, either high bottom or high wall heating. The generalized exit temperature histories for each type of heating are presented in figure 7. The heating parameter $\dot{\mathcal{Q}}$ is shown for each case. Increasing the initial heating rate to

the system with the same flow rate and tank pressure results in higher values of the heating parameter $\dot{\mathcal{Q}}$. As expected, increasing this parameter increased the rate of exit temperature rise for either type of heat input distribution. With high bottom heating a greater portion of the initial heating rate enters the liquid for a longer period of time than with high wall heating (fig. 6). Consequently, exit temperatures with high bottom heating (fig. 7(a)) are greater than those with high wall heating (fig. 7(b)) at any given time for about the same heating parameter $\dot{\mathcal{Q}}$.

Neither the wall nor the bottom heating data (fig. 7) are strictly families of curves since the heating rate distributions differ slightly with each type of heating (fig. 6) in addition to variations in the heating parameter. For this reason, caution should be exercised in interpolating these data to intermediate values of heating parameter.

Comparison of Bottom and Nuclear Heating Data

A typical generalized heating distribution curve from the nuclear heating data of reference 8 was presented in figure 6. The shape of this curve is similar to those of the present data having high bottom heating. It was considered of interest, therefore, to compare the present bottom heating data with the nuclear heating data. The nuclear heating rate distribution was essentially independent of initial heating rate, and consequently the generalized total heating rate distributions all had about the same shape. Therefore, the exit temperature histories should form a consistent family of curves with the heating parameter $\dot{\mathcal{Q}}$.

The generalized exit temperature histories of the nuclear heating data are presented in figure 8. Also shown are the corresponding operating conditions for each test run and the heating parameter $\dot{\mathcal{Q}}$. The several test runs have been presented in the order of decreasing values of the heating parameter. Four test runs yielded heating parameters from 0.373 to 0.388, which covered a range of two in pressure level and in initial total heating rate. In another instance, heating parameters of 0.117 and 0.120 occurred with the effect of initial total heating rate variations approximately balanced by changes in tank pressure and flow rate. In both instances, the generalized exit temperature histories were consistent showing that the heating parameter adequately accounted for changes in operating conditions.

A comparison of the bottom heating data with the nuclear data (figs. 7(a) and (8)) shows consistent generalized exit temperature histories with the parameter $\dot{\mathcal{Q}}$. The L - ML configuration of figure 7(a) had a heat input rate distribution most similar to the nuclear data. In this instance, the shape of the generalized exit temperature history ($\dot{\mathcal{Q}} = 0.117$) bears a striking resemblance to a nuclear data run having the same value of $\dot{\mathcal{Q}}$. The same value of $\dot{\mathcal{Q}}$ was achieved in the nuclear data run with a greater initial heat input rate but with a compensating higher flow rate and tank pressure. Perhaps the

most significant factor of the comparison of bottom and nuclear heating is that the approach of simulating nuclear heating by bottom heating appears to be feasible.

SUMMARY OF RESULTS

The following results were obtained from an experimental study of the behavior of liquid hydrogen contained in a tank subjected to wall and bottom heating during flow at constant pressure:

1. Increasing the wall heat flux with low bottom heat flux showed that the added heat accumulated in a stratified layer. A decrease in stratification occurred when the bottom heat flux was increased with a trend toward a completely mixed condition except for a thin surface layer.

2. No gross changes in liquid behavior were experienced over the range of experimental conditions.

3. An available analysis partially predicted the increase in temperature stratification with increasing wall heat flux. The general agreement between the predicted and measured temperatures may be useful to interpolate between experimental results.

4. A set of dimensionless parameters was derived to obtain generalized exit temperature histories. Use of the parameters showed that the data can be made applicable to other test conditions provided similar heat input rate configurations are used.

5. Application of the generalization method to other test data showed that bottom heating gave exit temperature histories similar to nuclear heating from below with similar overall heat input rate distribution.

Lewis Research Center,
National Aeronautics and Space Administration,
Cleveland, Ohio, November 23, 1965.

APPENDIX A

SYMBOLS

A	tank cross-sectional area
c_p	specific heat at constant pressure
E	interchange factor, liquid energy
e	energy per unit mass
$f(t)$	ratio of exit temperature rise to saturation temperature rise
h_v	heat of vaporization
L	initial height of liquid
n	exponent, eq. (D2)
P_n	heating rate per unit volume
P_T	tank pressure
$\dot{Q}$	heating rate
$\dot{\mathscr{Q}}$	heating parameter, ratio of initial heating rate to saturation heating rate, eq. (7)
$\dot{Q}_H$	heating rate from heaters, eq. (1)
$\dot{Q}_\ell$	heating rate of liquid, eq. (3)
$\dot{Q}_s$	saturation heating rate, eq. (6)
q	heat flux
r	radius
r_o	radius of tank bottom
S	surface area of tank
S_i	surface area of tank from $x = 13.5$ to x_i
T	temperature
t	time
V	volume
$\dot{V}$	volumetric flow rate
v	ratio of volume to initial volume of fluid
$\dot{w}$	weight flow rate
x	axial distance from tank bottom
δ	thickness of stratified layer
ϵ	emissivity
ϑ	ratio of temperature difference to saturation temperature difference
ρ	fluid density
σ	Stefan-Boltzmann constant
τ	ratio of time to time to outflow, t/t_m
ψ	similarity parameter, eq. (D2)

Subscripts:

1, 2, 3	tangent points
H	heater
i	bottom of stratified layer
in	initial condition
ℓ	liquid
m	maximum
s	saturation, surface condition
T	tank
w	wall
sl	stratified layer

Superscript:

$\bar{}$	average conditions

APPENDIX B

DESCRIPTION OF TEST APPARATUS, INSTRUMENTATION, AND PROCEDURE

Tank

The tank, constructed of 304 stainless steel, had a liquid capacity of about 125 gallons. The tank geometry consisted of a 32-inch-diameter cylinder mounted on top of a spherical zone transition to the frustrum of a 45° half angle cone on a spherical segment (see table II). A 3/4-inch schedule 40 liquid outflow pipe extended below the tank. The tank skin was 1/8 inch in thickness. A flange and transition section were located at the upper end of the cylinder to permit removal of the tank from the hemispherical top. The outer surface of the tank (and the inner surface of both the wall and bottom heaters) was sand blasted and spray painted with a flat black lacquer to provide a high emissivity surface.

A window-type opening was available in the side of the tank, but it was sealed with a steel cover for this set of experiments (fig. 2). Two similar ports installed in the tank dome were used for the purposes of viewing and illumination of the tank interior.

Radiant Heaters

The radiant heaters were constructed from 304 stainless steel ribbons. The wall heater consisted of a double lead coil of 1- by 1/16-inch ribbon cylindrically wrapped with a $37\frac{1}{2}$-inch inside diameter and a $2\frac{1}{4}$-inch pitch. Each coil had approximately 13 convolutions. The bottom ends of each coil were joined with a $2\frac{1}{4}$-inch strip of the heater material to form one continuous strip to which electrical power leads were attached at each end. A 13-inch-diameter opening had to be provided for the protruding flange on the side of the tank. Sections of the ribbons were removed to provide the opening, but the concept of a continuous strip was maintained by rejoining appropriate bands (see fig. 2). The overall height of the wall heater was about 30 inches. Integrity of the coil was maintained by using vertical insulating bars riveted to each ribbon. The bars also provided a means of supporting the heaters from the top of the vacuum jacket while maintaining both electrical and thermal barriers.

The bottom heater consisted of a double lead coil of 3/4 by 1/16 inch ribbon helically wrapped with a 45° half angle from the axis with a major diameter of $36\frac{3}{4}$ inches using a

$1\frac{3}{4}$-inch pitch. Each coil had approximately 13 convolutions with the bottom lead ends joined to form one continuous strip. The bottom heater was suspended from the wall heater by using similar bars for support and integrity as in the case of the wall heater.

The double lead coils of one continuous strip were used for both the wall and bottom heaters to prevent inductive coupling between the heaters and the tank. Voltage regulated alternating current was separately supplied to each heater.

Instrumentation

Two temperature measurement systems were used for the test; one consisted of carbon resistors to measure temperatures in the cryogenic temperature range and the other of copper constantan thermocouples to measure temperature above cryogenic temperatures. The temperature measurement positions are shown in table III. Thirty carbon-resistor thermometers were mounted on a rake extending down the tank axis. These thermometers were spaced at 1/4-inch increments near the liquid surface of the full tank at the 4-inch increments otherwise. A thermometer placed at the tank exit was used to observe the liquid temperature leaving the tank. Eight additional thermometers were mounted radially 1/8 inch and 1/4 inch off the tank wall. The 100-ohm, 1/10-watt resistors were mounted in a horizontal position. Thirty-six copper constantan thermocouples, mounted along the entire axis of the tank at 4 inch or less increments on the axial rake, were used to observe gas temperatures. The thermocouples were spaced at 1/4-inch increments near the surface of the full tank and near the surface of the half-full tank. Four additional thermocouples were mounted radially 1/8 inch and 1/4 inch off the tank wall. Six thermocouples were attached to the outer wall of the test tank to measure tank wall temperatures. Three thermocouples were attached to the inner surface of each radiant heater to measure the heater temperature.

The response time of both the carbon resistor thermometers and the thermocouples was expected to be at least 2 seconds. Previous experience with this type of carbon resistor gave indication that an accuracy within 0.1° R was obtainable in the range of liquid hydrogen temperatures. The thermocouple accuracy was estimated to be within 1° R at temperature levels greater than 138° R. (An atmospheric liquid nitrogen reference bath was used for the thermocouples.)

A strain-gage type pressure transducer was used to measure tank pressure. A venturi, installed in a vacuum chamber several pipe diameters downstream of the tank shutoff valve, together with an upstream pressure transducer, a differential pressure transducer, and a downstream carbon resistor thermometer were used to indicate the liquid flow rate.

Test Procedure

The general procedure of the investigation was to first establish a heating configuration consisting of a particular wall heat flux and a particular bottom heat flux into the test tank. With each configuration, a flow test was conducted which consisted of filling the tank with liquid hydrogen, pressurizing to about 2 atmospheres, and then maintaining the pressure constant during outflow at a rate of about 0.04 pound per second. The flow test conditions for each configuration are presented in table I.

Boiloff and no-flow tests were performed to check the method of obtaining the heat input rate distribution. Boiloff tests were performed in which the tank, filled with liquid hydrogen, was allowed to vent at a constant tank pressure. During these tests the liquid level history was obtained.

No-flow tests were performed which consisted of establishing a given heating configuration with the tank vented after which the fill and vent valves (see fig. 1) were closed; this allowed the tank to pressurize. The liquid temperature and tank pressure history were used to determine the heat input rate associated with a particular mass of liquid.

The double wall of the outer shell (see fig. 1) was filled with liquid nitrogen to ensure a constant reproducible wall temperature which would yield a low ambient heat leak. To decrease the heat leak from the flanges, a tub-like structure was built around the exit port and filled with liquid nitrogen.

Prior to the start of the flow tests, the throttle valve was opened and liquid hydrogen from the supply dewar was flowed through to chill the venturi for approximately 15 minutes prior to start of outflow from the tank. At this time, the throttle valve was adjusted to yield the desired flow rate. About 20 seconds prior to start of flow, the tank was pressurized with hydrogen gas to 1 atmosphere above the initial pressure level. (Prior to tank pressurization, the liquid contents were at saturation temperature corresponding to the initial pressure.) Next, the fill valve was closed. A few seconds after the tank had achieved stable pressure, the shutoff valve was opened and the flow of hydrogen began. Additional pressurizing gas was used as needed to maintain a constant tank pressure during the entire flow run. The pressurant was introduced into the tank through a gas diffuser to avoid disturbing the liquid surface.

APPENDIX C

HEAT INPUT RATE DISTRIBUTION

Heat Input From Radiant Heaters

Preliminary runs with the test apparatus indicated a problem not previously anticipated. Cooldown of the radiant heaters resulted in a temperature gradient in each heater in the vertical direction. The low value of thermal conductivity of the 304 stainless steel heater, combined with the long length of each coil, required an excessive time period to equalize the temperature throughout either heater. Therefore, a simple thermal radiation calculation was used to account for the variation in heating rate resulting from the temperature differences.

Each heater was considered to consist of three zones, each zone having a uniform temperature measured by the thermocouple in the zone. The net radiant heat exchange was then calculated between each zone of a heater and the corresponding tank surface, assuming that both the heater and the wall were gray surfaces and the close spacing of the heater to the tank wall was analogous to concentric cylinders. The net heat exchange per unit tank area per unit time from each zone was then computed from the equation

$$q = \sigma E(T_H^4 - T_T^4) \tag{C1}$$

where σ is the Stefan-Boltzmann constant and

$$\frac{1}{E} = \frac{1}{\epsilon_T} + \frac{r_T}{r_H}\left(\frac{1}{\epsilon_H} - 1\right)$$

Constant emissivities of 0.8 were assumed for both surfaces. The net heat input rate to the liquid from the heaters was then obtained from the equation

$$\dot{Q}_H(x_s) = \int_0^{x_s} q \frac{dS}{dx}\, dx \tag{C2}$$

where q is obtained from equation (C1) and x_s is the height of liquid in the tank.

Boiloff Tests

A boiloff test was conducted in which the liquid level history was measured during the time required to completely boil off the initial tank contents. The heat input rate from the heaters was also calculated for this test in the manner previously described (eq. (C2)) by using the measured heater temperatures. This heat input rate from the heaters was used to calculate the time required to boil off a given height of liquid. The equation used for this calculation was

$$t = \int_{x_s}^{L} \frac{h_v \rho A(x_s)}{\dot{Q}_H(x_s)} dx_s \tag{C3}$$

The heat input rate to the liquid during the boiloff test was calculated from the measured liquid level history using the rate of change of liquid height in the expression

$$\dot{Q}_\ell = h_v \rho A(x_s) \frac{dx_s}{dt} \tag{C4}$$

The experimental results of the boiloff test are presented in figure 9 as the history of liquid height. Also shown is the calculated history of liquid height based on the heat input from the radiant heaters obtained from equation (C3). A comparison between the two curves indicates the method used to calculate the heat input rate from the radiant heaters, when applied in this manner, resulted in predicting within 5 percent the time required to completely boil off the initial tank contents. The heat input rate distribution calculated from the radiant heater method (eq. (C2)) is presented in figure 10 as a function of liquid height. Also shown is the calculated heat input rate to the liquid obtained from using the observed history of liquid height (eq. (C4)). The two methods of calculating heat input distribution were considered to agree satisfactorily within the accuracy of measurement. At a height of 45 inches, the liquid heating rate showed about 10-percent higher power level than indicated by the heater calculation. This test was conducted at a high power level (1 kW into the full tank) to keep the test duration within a reasonable time period.

No-Flow Tests

No-flow tests were conducted to check the method of calculating the heat input rate from the radiant heaters. The test conditions for the no-flow tests are summarized in

table IV. In a few instances, two tests were conducted using the same heating configuration but with different initial heights of liquid to check heat distribution.

The energy of the liquid at a given time t during a no-flow (or self-pressurizing) test was calculated from the equation

$$E(t) = \int_0^{x_s} \rho(x, t) e(x, t) A(x)\, dx$$

where the local density $\rho(x, t)$ and specific energy $e(x, t)$ were obtained from National Bureau of Standards literature as a function of tank pressure P_T and a local axial liquid temperature $T(x, t)$. At a given time, the temperature data was curve-fit using a three-point, one-slope fit for each region defined by thermometer locations. An average heating rate of the liquid (third column of table IV) was then calculated from the equation

$$\dot{\bar{Q}}_\ell = \frac{E(t_m) - E(o)}{t_m}$$

The heater temperatures deviated a small amount during the course of a test. An average heat input rate from the radiant heaters (fourth column of table IV) was therefore used to account for this slight deviation. The equation used to obtain this average heat input rate was

$$\dot{\bar{Q}}_H = \frac{1}{t_m} \int_0^{t_m} \int_0^{x_s(t)} q(x) \frac{dS}{dx}\, dx\, dt$$

where $q(x)$ was obtained from equation (C1) and the time period of the no-flow test t_m (fifth column of table IV).

The average heat input rate from the heaters was consistently less than the average heating rate of the liquid (table IV). The heating error defined by the ratio $(\dot{\bar{Q}}_\ell - \dot{\bar{Q}}_H)/\dot{\bar{Q}}_H$ is presented in figure 11 as a function of the average heat input rate $\dot{\bar{Q}}_H$. Also shown is a dashed curve representing a constant difference of 30 watts. The dashed curve represents a mean average of the experimental data within the accuracy of measurement. The general consistency between the heating errors for both heights of liquid with the same configuration was considered sufficient evidence to warrant using the radiant heat calculation method as a means of determining the heat input rate distribution.

APPENDIX D

APPLICATION OF ANALYSIS

A method for the analytical prediction of liquid temperature history subjected to heating during flow from the propellant tank at a constant flow rate and pressure was developed in reference 9. The use of the method requires a knowledge of tank geometry, test conditions, liquid properties, heat input distribution, and assumptions regarding the manner in which the heat input will influence the liquid behavior. Some of the basic equations used in reference 9 are presented herein for completeness, and the application of the analysis to the present data is presented. The system was considered to include only the liquid in the tank while discharging at constant pressure and flow rate. The boundary conditions included heat transfer from the walls, the surface temperature (corresponding to tank pressure), and heat added to the system by the absorption of nuclear radiation. The analytical flow model consisted of a lower region of completely mixed liquid with an upper region of stratified liquid having a temperature gradient extending from the completely mixed liquid temperature to saturation temperature at the surface.

The basis for the flow model of the analysis was to treat the nuclear heating in the liquid and a portion of the heat transfer from the bottom section of the tank as though it resulted in completely mixing the liquid in the region below the stratified layer. The heat transfer along the vertical walls was then considered to form the stratified layer, which was assumed to have the property of similarity (that is, the property that two temperature profiles $\Delta T(x, t)$ at different times differ only in a scale factor in x and ΔT). By this assumption, the temperature in the stratified layer can be written in the form

$$\Delta T(x, t) = \Delta T_s \left\{ f(t) \left[1 - \psi(x, t) \right] + \psi(x, t) \right\} \tag{D1}$$

where $\psi(x, t)$ is the similarity parameter and the parameter $f(t)\left[1 - \psi(x, t)\right]$ can be interpreted as the necessary contribution of nuclear (and bottom) heating in the stratified layer to preserve the condition of similarity. By specifying that the parameter ψ identically vanishes below the stratified layer, equation (D1) can be used as the dimensionless profile for the entire fluid. It is apparent that ψ must also satisfy the condition that at the liquid surface $\psi = 1$. It was found in reference 9 that under the conditions where the side wall heating was small relative to nuclear (and bottom) heating, the parameter $\psi(x, t)$ may be approximated by the form

$$\psi(x, t) = \left[\frac{x - x_i(t)}{\delta(t)} \right]^n \tag{D2}$$

where $x_i(t)$ is the lower extremity of the stratified layer and $\delta(t)$ is the thickness of the stratified layer. To determine the three unknowns, f(t), $\delta(t)$, and the exponent n, the energy equation of the system and the assumed energy balance between the boundary and the wall heating of the forms

$$\rho c_p \frac{d}{dt}\int_V \Delta T\, dV + c_p \dot{w}\, \Delta T(o, t) = \int_S q_w\, dS + \int_V P_n\, dV \tag{D3}$$

$$\rho c_p\, \overline{\Delta T}_w \frac{d}{dt}\int_{V_{s\ell}} dV = \int_{S_i} q_w\, dS \tag{D4}$$

were used. The assumption was made that the contributions of side wall heating and nuclear heating (including bottom heating) could be uncoupled. When equation (D1) is substituted into (D3), the uncoupling results in

$$\rho c_p\, \Delta T_s \frac{d}{dt}\int_V f(t)(1 - \psi)\, dV + c_p \dot{w}\, \Delta T_s\, f(t) = \int_V P_n\, dV \tag{D5}$$

$$\rho c_p\, \Delta T_s \frac{d}{dt}\int_V \psi\, dV = \int_S q_w\, dS \tag{D6}$$

The system of equations (D4), (D5), and (D6) was then solved for the unknown quantities f(t), $\delta(t)$, and the exponent n.

For the comparison of analysis and experimental data presented herein, the volume integral on the right hand side of equation (D5) was replaced by a surface integral of heat flux over the tank bottom. The same assumption was made (as in ref. 9) that all heat input below the point x = 13.5 inches would be assigned to bottom heating. In a like manner, all heat input above the point x = 13, 5 inches was assigned to the side wall heating.

The right hand side of equation (D5) then becomes

$$\int_V P_n\, dV = \dot{Q}_\ell(13.5) \qquad 13.5 \leq x_s \leq L$$

$$= \dot{Q}_\ell(x_s) \qquad 0 \leq x_s < 13.5$$

and similarily, the right hand side of equation (D6) becomes

$$\int_S q_w \, dS = \dot{Q}_\ell(x_s) - \dot{Q}_\ell(13.5) \qquad 13.5 \leq x_s \leq L$$

$$= 0 \qquad 0 \leq x_s < 13.5$$

where $\dot{Q}_\ell(x_s)$ is obtained using equation (4).

An average wall heat flux $\bar{q}_w$ required for the evaluation of the exponent n (see ref. 9) was then obtained from the relation

$$\bar{q}_w = \frac{\dot{Q}_\ell(L) - \dot{Q}_\ell(13.5)}{S(L) - S(13.5)}$$

where the surface area S was calculated from the tank geometry.

REFERENCES

1. Barnett, D. O.; Winstead, T. W.; and McReynolds, L. S.: An Investigation of Liquid-Hydrogen Stratification in a Large Cylindrical Tank of the Saturn Configuration. Advances in Cryogenic Engineering, vol. 10. Sec. M-U, K. D. Timmerhaus, ed., Plenum Press, 1965, pp. 314-324.

2. Segel, M. P.: Experimental Study of the Phenomena of Stratification and Pressurization of Liquid Hydrogen. Advances in Cryogenic Engineering, vol. 10, Sec. M-U, K. D. Timmerhaus, ed., Plenum Press, 1965, pp. 308-313.

3. Tatom, J. W.; Brown, W. H.; Knight, L. H.; and Coxe, E. F.: Analysis of Thermal Stratification of Liquid Hydrogen in Rocket Propellant Tanks. Advances in Cryogenic Engineering, vol. 9, K. D. Timmerhaus, ed., Plenum Press, 1964, pp. 265-272.

4. Vliet, G. C.: Stratified Layer Flow Model - A Numerical Approach to Temperature Stratification in Liquids Contained in Heated Vessels. Lockheed Missiles and Space Co., Palo Alto, Calif., Aerospace Sciences Lab., Nov. 1963.

5. Robbins, J. H.; and Rogers, A. C., Jr.: An Analysis on Predicting Thermal Stratification in Liquid Hydrogen. Paper No. 64-426, AIAA, June-July 1964.

6. Anderson, Bernhard H.; and Kolar, Michael J.: Experimental Investigation of the Behavior of a Confined Fluid Subjected to Nonuniform Source and Wall Heating. NASA TN D-2079, 1963.

7. Clark, J. A.: A Review of Pressurization, Stratification and Interfacial Phenomena. Advances in Cryogenic Engineering, vol. 10, Sec. M-U, K. D. Timmerhaus, ed., Plenum Press, 1965, pp. 259-283.

8. Hehs, W. A.; McCauley, B. O.; Miller, G. E.; and Wheeler, D. M.: Nuclear Radiation Heating in Liquid Hydrogen. Vol. 1 - Description and Experiment and Discussion of Results. NASA CR-54078, 1964.

9. Anderson, Bernhard H.; and Danilowicz, Ronald L.: Analytical and Experimental Study of Nuclear Heating of Liquid Hydrogen. NASA TN D-2934, 1965.

TABLE I. - FLOW TEST CONDITIONS

[a]Heat flux configuration	Average wall heat flux, Btu/(sq ft)(sec)	Average bottom heat flux, Btu/(sq ft)(sec)	Initial height of liquid, L, in.	Initial temperature, T_{in}, ^{o}R	Tank pressure, P_T, psia	Saturation temperature rise, ΔT_S, ^{o}R	Flow rate, $\dot{w}$, lb/sec	Average specific heat, $\bar{c}_p$, Btu/(lb)(^{o}R)	Average density, $\bar{\rho}$, lb/cu ft	Average heating rate ratio, $\dot{\bar{Q}}_\ell/\dot{\bar{Q}}_H$
L - L	2.81×10^{-3}	1.10×10^{-3}	44.5	38.70	33.39	3.41	0.0405	2.45	4.32	6.840
ML - L	4.07	.45	45.1	38.32	34.40	4.02	.0417	2.45	4.33	2.890
MH - L	6.37	.53	46.1	38.39	33.40	3.95	.0424	2.48	4.32	1.519
H - L	7.19	.52	44.7	38.44	34.22	3.63	.0411	2.50	4.31	1.204
L - ML	1.05	3.61	45.1	38.28	34.40	4.06	.0410	2.45	4.33	2.617
L - MH	1.22	4.94	44.3	38.16	34.31	4.16	.0407	2.45	4.33	1.613
L - H	1.74	9.75	44.7	38.40	34.40	3.94	.0415	2.50	4.30	1.577
H - H	8.23	7.48	44.2	38.45	34.40	3.89	.0416	2.53	4.29	1.144

[a]Average wall heat flux - average bottom heat flux: H, high; L, low; ML or MH, intermediate values.

TABLE II. - TANK GEOMETRY

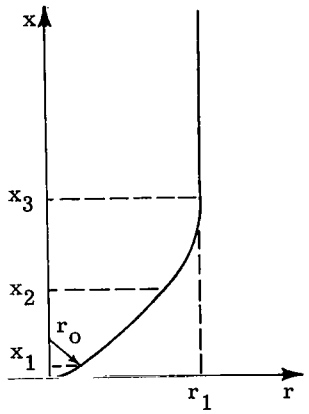

r_o = 4.83 in.
r_1 = 16 in.
x_1 = 1.41 in.
x_2 = 9.31 in.
x_3 = 20.62 in.

[a]Region	Equation of tank profile	Geometry
$0 \leq x \leq x_1$	$r(x) = \left[-x^2 + 2r_o x\right]^{1/2}$	Sphere
$x_1 \leq x \leq x_2$	$r(x) = x + 2$	Cone
$x_2 \leq x \leq x_3$	$r(x) = \left[-x^2 + 2x_3 x + (r_1^2 - x_3^2)\right]^{1/2}$	Sphere
$x_3 \leq x \leq L$	$r(x) = r_1$	Cylinder

[a]Regions are distinguished by tangent points.

TABLE III. - LOCATION OF TEMPERATURE PROBES

Height from bottom of tank, in.	Probe location								Height from bottom of tank, in.	Probe location							
	Carbon resistor			Thermocouple						Carbon resistor			Thermocouple				
	Axial	Radial distance from wall, in.		Axial	Radial distance from wall, in.		Outer wall	Radiant heater		Axial	Radial distance from wall, in.		Axial	Radial distance from wall, in.		Outer wall	Radiant heater
		0.125	0.25		0.125	0.25					0.125	0.25		0.125	0.25		
0	x								$41\frac{11}{16}$	x							
$\frac{7}{8}$	x	x	x	x			x	x	$41\frac{15}{16}$	x							
$4\frac{7}{8}$	x			x					$42\frac{3}{16}$	x							
$8\frac{7}{8}$	x	x	x	x			x	x	$42\frac{7}{16}$	x							
$12\frac{7}{8}$	x			x					$42\frac{11}{16}$	x							
$15\frac{3}{16}$								x	$42\frac{15}{16}$	x							
$16\frac{7}{8}$	x	x	x	x			x	x	$43\frac{3}{16}$	x							
$20\frac{11}{16}$	x			x					$43\frac{7}{16}$	x							
$24\frac{11}{16}$	x			x					$43\frac{11}{16}$	x	x	x					
$24\frac{15}{16}$	x			x					$43\frac{15}{16}$	x							
$25\frac{3}{16}$	x			x					$44\frac{3}{16}$	x			x				
$25\frac{7}{16}$	x			x					$44\frac{7}{16}$	x			x				
$25\frac{11}{16}$				x					$44\frac{11}{16}$	x			x	x	x	x	x
$25\frac{15}{16}$				x	x	x	x		$44\frac{15}{16}$				x				
$26\frac{3}{16}$				x					$45\frac{3}{16}$				x				
$26\frac{7}{16}$				x					$45\frac{7}{16}$				x				
$26\frac{11}{16}$				x					$45\frac{11}{16}$				x				
$27\frac{11}{16}$				x					$45\frac{15}{16}$				x				
$28\frac{11}{16}$				x					$46\frac{3}{16}$				x				
$32\frac{11}{16}$	x			x			x	x	$47\frac{3}{16}$				x				
$36\frac{11}{16}$	x			x					$48\frac{3}{16}$				x				
$40\frac{11}{16}$	x			x					$50\frac{3}{16}$				x				
$40\frac{15}{16}$	x								$52\frac{3}{16}$				x				
$41\frac{3}{16}$	x								$54\frac{3}{16}$				x				
$41\frac{7}{16}$	x								$56\frac{3}{16}$				x				
									$58\frac{3}{16}$				x				

TABLE IV. - NO-FLOW TEST CONDITIONS

[a]Heat flux configuration	Initial height of liquid, L, in.	Average heating rate of liquid, $\dot{\overline{Q}}_{\ell}$, W	Average heat input rate from heaters, $\dot{\overline{Q}}_{H}$, W	Time period, t_m, sec
L - L	42.7	35.5	4.0	2290
H - L	42.3	174.6	132.0	1155
L - H	41.7	113.4	68.2	2000
L - H	26.0	100.4	64.4	1740
H - H	42.0	223.3	195.0	1680
H - H	24.9	107.9	100.2	1680

[a]Average wall heat flux - average bottom heat flux: H, high; L, low; ML or MH, intermediate values.

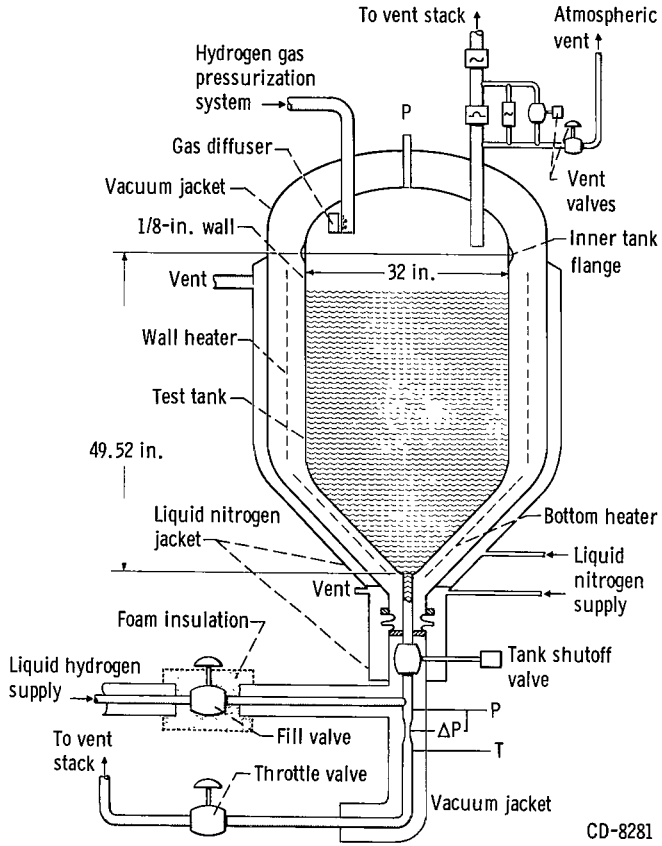

Figure 1. - Schematic of system.

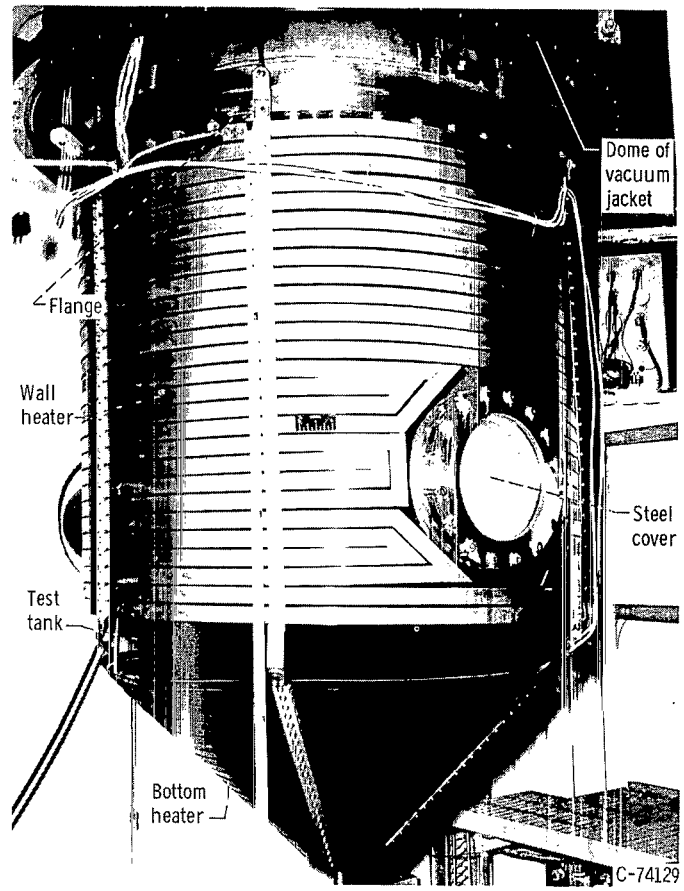

Figure 2. - Test tank with radiant heaters installed.

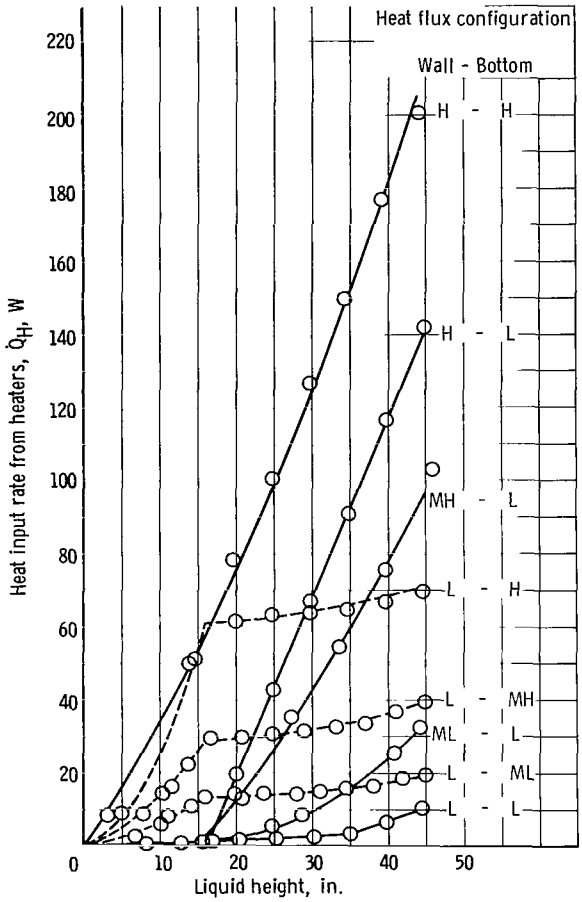

Figure 3. - Heat input rate distribution calculated from heaters.

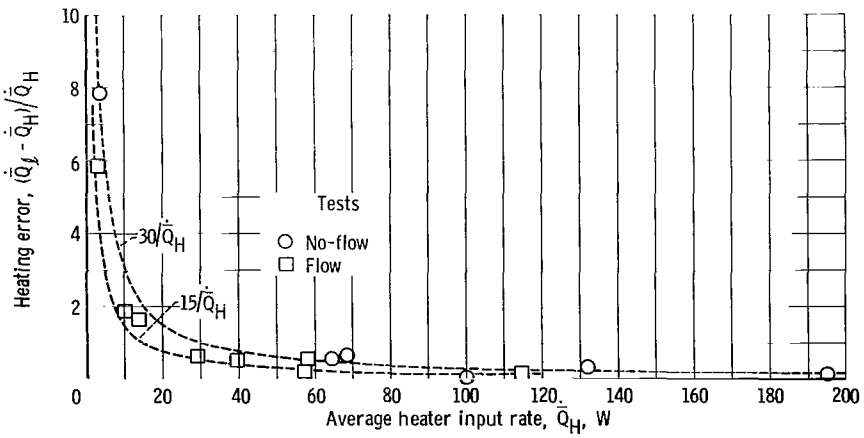

Figure 4. - Comparison of total heating rate of liquid with calculated heater input rate for no-flow and flow tests.

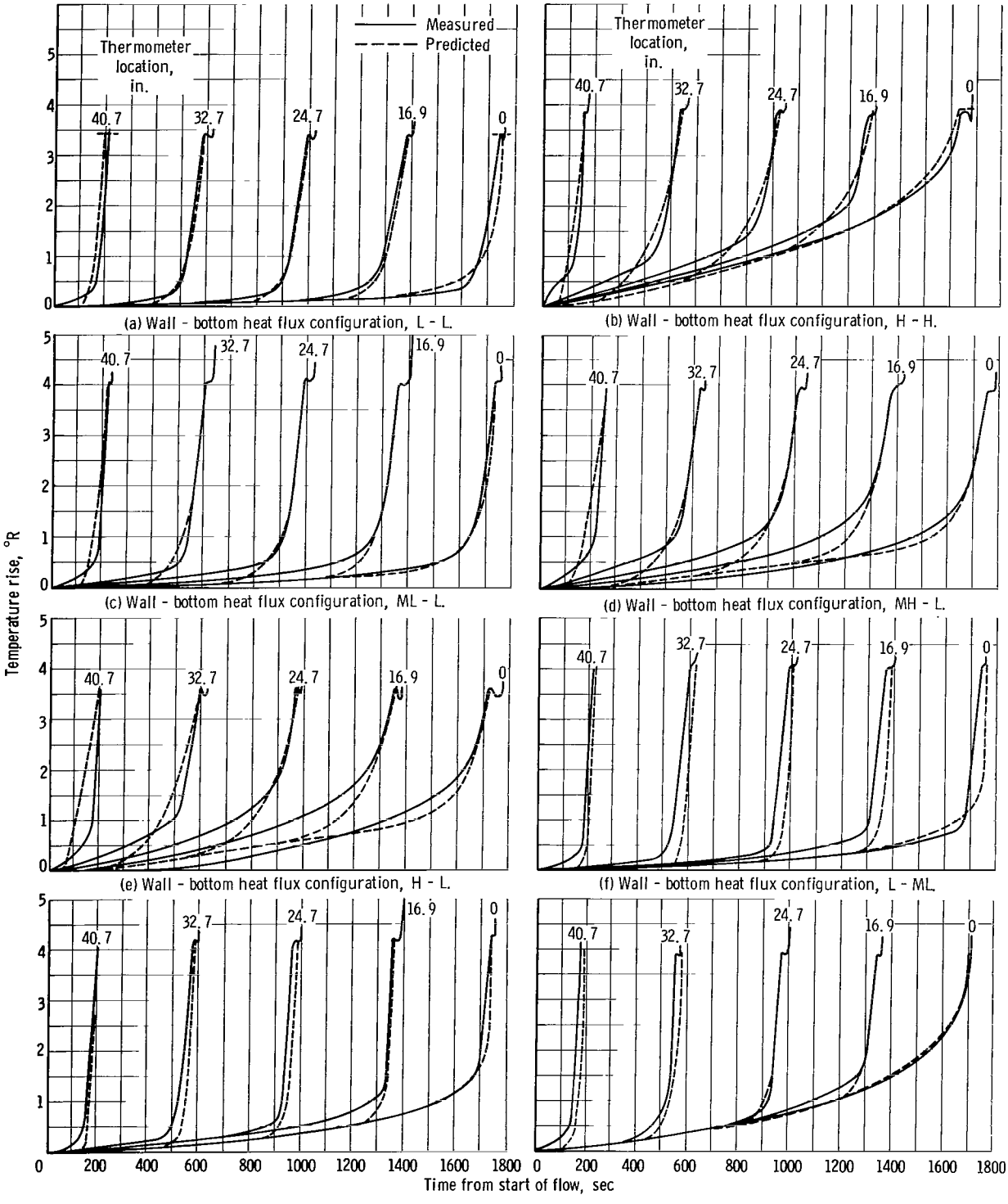

Figure 5. - Comparison of measured and predicted liquid hydrogen temperature histories at several thermometer locations during outflow.

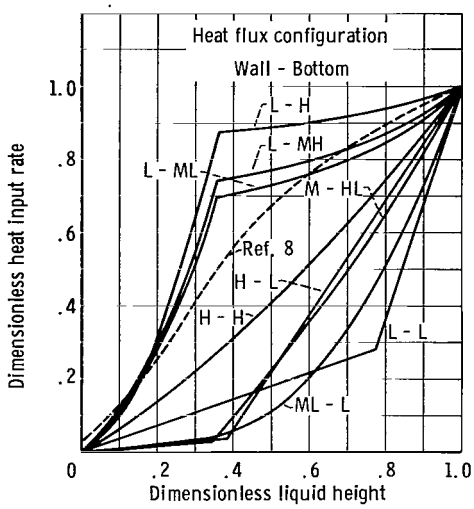

Figure 6. - Generalized heat input rate distribution.

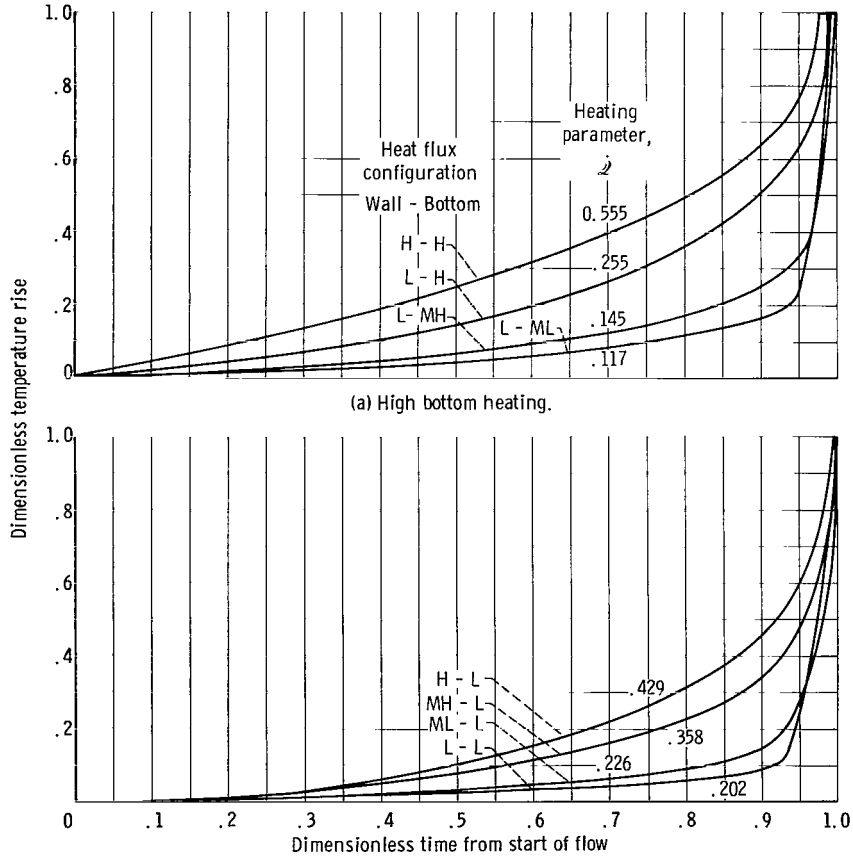

(a) High bottom heating.

(b) High wall heating.

Figure 7. - Generalized exit temperature histories of wall and bottom heating data.

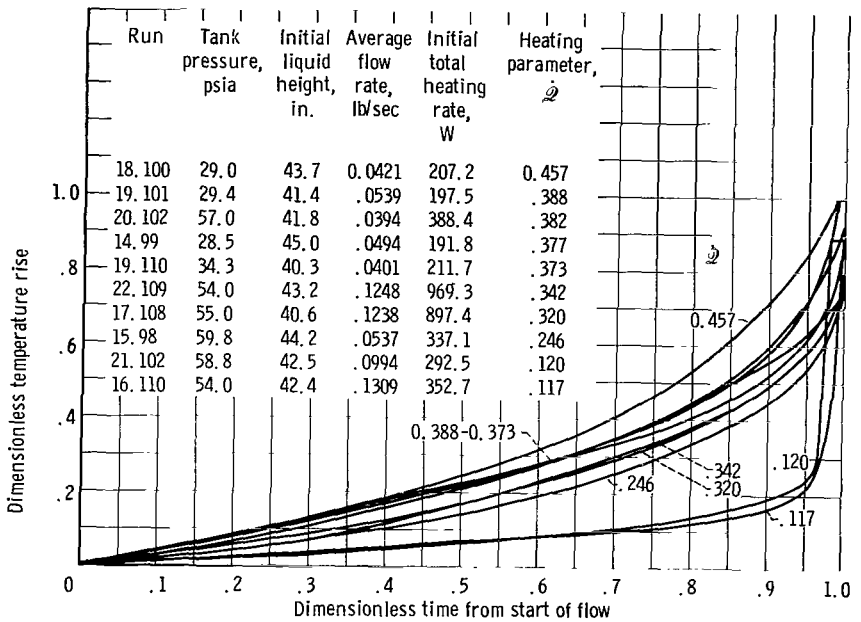

Figure 8. - Generalized exit temperature histories of nuclear heating data from reference 8.

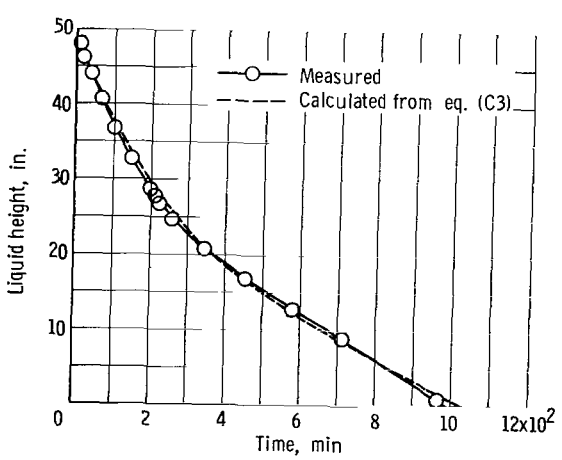

Figure 9. - Liquid level history during boiloff test.

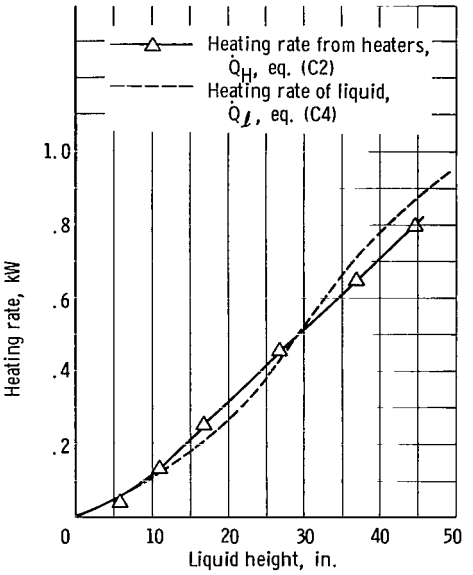

Figure 10. - Heat input rate distribution for boiloff test.

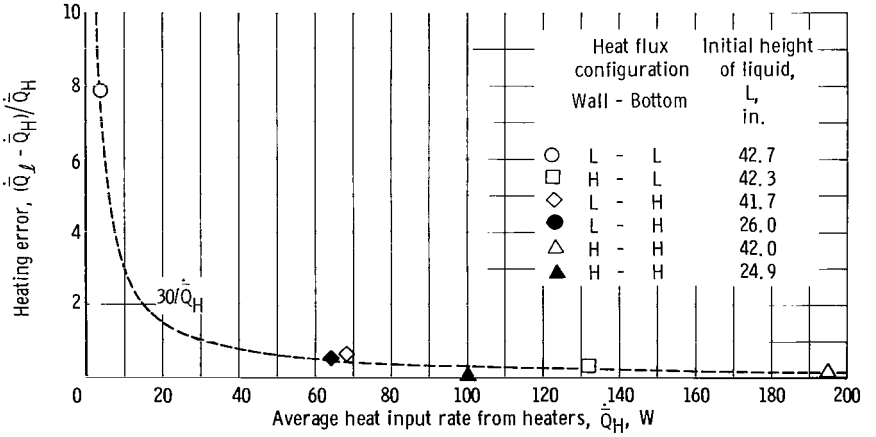

Figure 11. - Comparison of heating rate of liquid with heat input rate from heaters for no-flow tests.

"The aeronautical and space activities of the United States shall be conducted so as to contribute . . . to the expansion of human knowledge of phenomena in the atmosphere and space. The Administration shall provide for the widest practicable and appropriate dissemination of information concerning its activities and the results thereof."

—NATIONAL AERONAUTICS AND SPACE ACT OF 1958

NASA SCIENTIFIC AND TECHNICAL PUBLICATIONS

TECHNICAL REPORTS: Scientific and technical information considered important, complete, and a lasting contribution to existing knowledge.

TECHNICAL NOTES: Information less broad in scope but nevertheless of importance as a contribution to existing knowledge.

TECHNICAL MEMORANDUMS: Information receiving limited distribution because of preliminary data, security classification, or other reasons.

CONTRACTOR REPORTS: Technical information generated in connection with a NASA contract or grant and released under NASA auspices.

TECHNICAL TRANSLATIONS: Information published in a foreign language considered to merit NASA distribution in English.

TECHNICAL REPRINTS: Information derived from NASA activities and initially published in the form of journal articles.

SPECIAL PUBLICATIONS: Information derived from or of value to NASA activities but not necessarily reporting the results of individual NASA-programmed scientific efforts. Publications include conference proceedings, monographs, data compilations, handbooks, sourcebooks, and special bibliographies.

Details on the availability of these publications may be obtained from:

SCIENTIFIC AND TECHNICAL INFORMATION DIVISION

NATIONAL AERONAUTICS AND SPACE ADMINISTRATION

Washington, D.C. 20546